

Spiral Structures in an Embedded Protostellar Disk Driven by Envelope Accretion

Chin-Fei Lee^{1,2*}, Zhi-Yun Li³, & Neal J. Turner⁴

¹*Academia Sinica Institute of Astronomy and Astrophysics, P.O. Box 23-141, Taipei 106, Taiwan*

²*Graduate Institute of Astronomy and Astrophysics, National Taiwan University, No. 1, Sec. 4, Roosevelt Road, Taipei 10617, Taiwan*

³*Astronomy Department, University of Virginia, Charlottesville, VA 22904, USA*

⁴*Jet Propulsion Laboratory, California Institute of Technology, Pasadena, CA 91109, USA*

Hydrodynamical simulations show that a pair of spiral arms can form in the disk around a rapidly-growing young star and that the arms are crucial in transporting angular momentum as the disk accretes material from the surrounding envelope¹⁻⁴. Here we report the detection of a pair of symmetric spiral structures in a protostellar disk, supporting the formation of spiral arms in the disk around a forming star. The HH 111 VLA 1 source is a young Class I source embedded in a massive infalling protostellar envelope and is actively accreting, driving the prominent HH 111 jet. Previous observations showed a ring of shock emission around the disk's outer edge⁵, indicating accretion of the envelope material onto the disk at a high rate. Now with ALMA observations of thermal emission from dust particles, we detect a pair of spiral arms extending from the inner region to the disk's outer edge, similar to that seen in many simulations¹⁻⁴. Additionally, the disk is massive, with Toomre's Q parameter near unity in the outer parts where the spiral structures are detected, supporting the notion that

envelope accretion is driving the outer disk gravitationally unstable. In our observations, another source, HH 111 VLA 2, is spatially resolved for the first time, showing a disk-like structure with a diameter of ~ 26 au and an orientation nearly orthogonal to that of the HH 111 VLA 1 disk.

Spiral structures have been recently detected at (sub)millimeter wavelengths in protoplanetary disks whose protostellar envelopes have fully or partly dispersed⁶⁻⁹. These systems are in the late stages of their stars' growth, when planets are supposed to form. The spirals in most of these systems have $m = 2$ symmetry and trail relative to the disk rotation. The fact that systems are seen mostly with $m = 2$ structures could be due to observational bias since higher modes are harder to resolve¹⁰. Unlike the spirals detected in near-infrared and optical images that trace scattered star light, the (sub)millimeter spirals are thermal emission from dust that has settled closer to the midplane of the disk where the bulk of the mass resides, allowing us to investigate how the spirals are excited. The spirals could be induced by stellar or substellar companions, and thus potentially be linked to planet formation⁶⁻¹⁰. The spirals in some systems may be driven by global gravitational instability (GI)^{8,11,12}, in which the disks are massive enough that their self-gravity overcomes the thermal pressure and shear^{13,14}. Some of the spirals may be driven by both a companion and GI^{11,12}.

These spiral structures in protoplanetary disks near the end of star formation naturally raise the question of whether spiral structures can also appear in the early embedded phase of star formation when gas and dust from the surrounding molecular cloud core are still infalling onto the

disk. Indeed, a prominent spiral structure has been detected in the younger, Class 0 system L1448 IRS3B¹⁵. This is a triple system with a close binary at the center of the disk and a tertiary source in the outer disk. The disk in this system appears to have recently undergone GI, inducing the prominent spiral structure centered on the close binary with the third source located along the spiral structure in the outer disk¹⁵. The prominent spiral structure has apparently led to the formation of the tertiary source through disk fragmentation. When the disk gas has a cooling time shorter than about half the orbital period, the cooling can drive the disk toward instability and the collapse of one or more fragments to form new gravitationally-bound bodies^{2, 14}. Another potential example is the Class I binary system BHB07-11, where spiral-like structures are detected in dust continuum emission, although apparently in the inner protostellar envelope outside the compact circumbinary disk¹⁶.

Interestingly, many simulations have also shown that a pair of symmetric spiral structures can appear in the main protostellar mass accretion phase¹⁻⁴, starting from the Class 0 and persisting to the end of the Class I phase¹⁷. Unlike the spiral structure detected in L1448 IRS3B¹⁵, these are symmetric and play a critical role in transferring orbital angular momentum from the inner to the outer disk, allowing accretion even in the absence of other forms of angular momentum transport such as magneto-rotational instability or a disk wind¹⁸. In this paper, we report the detection of a pair of symmetric spiral structures in the protostellar disk of an embedded Class I source, in support of this possibility.

The HH 111 VLA 1 source is located in Orion at a distance of 400 pc. With a bolometric

temperature of only 78 K¹⁹, it is a Class I source and therefore young. It is still deeply embedded in a massive infalling envelope^{5,20}, and is both actively accreting and driving the prominent HH 111 jet that has a length of ~ 6.7 pc (at the remeasured distance)²¹. A rotating disk is detected toward the center with a radius of ~ 200 au^{5,20,22} producing polarized dust continuum emission²³. The central star has a mass $M_* \sim 1.5 \pm 0.5 M_\odot$ ^{5,20,22}. The infall rate in the envelope towards the center is estimated at $\sim 4.2 \times 10^{-6} M_\odot \text{ yr}^{-1}$ (20). Assuming mass flows at the same rate in the disk where $\sim 30\%$ of the flow is diverted into the jet and wind^{24,25}, the stellar accretion rate would be $\dot{M}_* \sim 2.9 \times 10^{-6} M_\odot \text{ yr}^{-1}$, resulting in an accretion age $M_*/\dot{M}_* \sim 5 \times 10^5$ yrs. Another source VLA 2 is also detected at a projected distance of ~ 1200 au to the west, forming a wide binary with the VLA 1 source.

Figure 1 presents our ALMA 343 GHz continuum map towards the two VLA sources at 0''04 (16 au) resolution, showing the thermal dust emission around them. The emission around the VLA 2 source is spatially resolved for the first time, appearing as a disklike structure, with a Gaussian deconvolved size (diameter) of 0''064 (25.6 au) along the major axis at position angle 118.3°. Since this disklike structure is roughly perpendicular to another jet, HH 121, the VLA 2 source likely drives the HH 121 jet, as suggested by observations of the CO outflow²⁶. Note that the VLA 2 disklike structure is nearly orthogonal to the VLA 1 disk, indicating the two components of this wide protobinary system are strongly misaligned.

The VLA 1 source powers the prominent HH 111 jet directed east-west, as indicated by the red and blue arrows. The surrounding emission shows a spatially resolved disk perpendicular to

the HH 111 jet, with its near side tilted to the southeast. To better see the disk structure, we rotate the disk to align its major axis with the vertical (Fig. 1b). As can be seen, the disk has a radius of $\sim 0''.4$ (160 au), where the rotation was previously found to be roughly Keplerian in C^{18}O ⁽⁵⁾. The aspect ratio of the disk structure is ~ 0.3 , indicating that the disk axis is inclined by $\sim 18^\circ$ to the plane of the sky, closely aligned with the HH 111 jet, which has an inclination angle of $13^\circ - 19^\circ$ (after the proper motion is updated for the new distance)²⁷.

Figure 1c shows the map deprojected by the inclination angle, revealing a roundish compact core and a pair of faint spiral structures in the outer disk. In order to better see the spirals, we first made an annularly averaged map of the continuum (see Figure 2b) then subtracted it from the deprojected map⁹. Figure 2c shows the difference map, which clearly shows a pair of symmetric spiral structures labeled “NE” and “SW” extending from within $\sim 0''.1$ (40 au) of the central source to the outer edge of the disk. To guide the eye, the emission peaks of the spirals are marked with green circles. As discussed in Methods, the positions of these emission peaks are obtained from Gaussian fits to the emission intensity in the radial direction. The spiral structures trail the rotation of the disk measured in molecular lines⁵. Near the central source, two barlike structures connect to the inner ends of the spiral structures. Since they are not clearly seen in the original map, these could be artifacts of the deprojection of the central region, which is spatially unresolved in the observation.

Two popular mechanisms have been proposed to account for the spiral structures in protoplanetary disks^{6,8}. One is the global GI due to the self-gravity of the disk itself, which can produce

a pair of symmetric, logarithmic spiral arms with a constant pitch angle¹². The other is a planet or a stellar companion, which can also induce one or more spirals but with the pitch angle increasing towards the location of the planet or companion^{12,28}.

Here we explore these two possibilities for the spiral arms in the deeply-embedded VLA 1 protostellar disk by studying their pitch angles. Figure 3 shows the two spiral arms, NE and SW, in polar coordinates, with R the radius and θ the polar angle. The data points correspond to the emission peaks in Figure 2c. We fitted the points with the two spiral shapes, one logarithmic with $R = R_0 \exp^{a\theta}$ and the other Archimedean with $R = R_0 + b\theta$, where b is the increase rate of the spiral radius with the angle, using the nonlinear least-squares Marquardt-Levenberg algorithm. Tables 1 and 2 list the fitting results with these two spiral structures. Based on the χ^2 values, it appears that the SW arm is slightly better fitted by a logarithmic shape, while the NE arm is slightly better fitted by an Archimedean shape. The pitch angle is $\sim 16^\circ$ for the SW arm and $\sim 13^\circ$ for the NE arm, both of which are similar to the pitch angle of the spirals in Elias 2-27 ($\sim 16^\circ$)⁸. Since neither shape fits both arms best, higher-resolution and deeper observations are needed to better distinguish these two possibilities.

Within the uncertainties of the current observations, the spiral structures in the VLA 1 disk are consistent with the logarithmic pattern expected from a global GI. The spiral structures are roughly symmetric and can be traced down to similar distance on opposite sides of the central source, also as expected for a global GI. Simulations of gravitationally unstable disks appear capable of reproducing the general morphology of the spiral structures in the VLA 1 disk^{10,17}. For

example, in the simulations of Tomida et al. (2017)¹⁷, the disk has a central core and an outer pair of symmetric spiral arms appearing in the outer part of the disk, resembling Figure 2c. Interestingly, in their simulations the spiral structures disappear and reform every few rotations as the disk accretes mass from the envelope and becomes unstable again. Such recurrent spiral arms first appear in the Class 0 phase and persist until accretion declines towards the end of the Class I phase. Spirals are expected to disappear soon after accretion has stopped²⁹. Accretion of envelope material onto the disk may trigger the development of spiral structures³⁰ and push power into lower- m modes⁴ even in non-self-gravitating disks.

Such recurrent spiral arms can also appear in the VLA 1 disk because the central source is still young and in the Class I phase. The source is deeply embedded in an envelope with a mass of $\sim 0.6 M_{\odot}$, extending out to ~ 7000 au from the VLA 1 source^{5,20}. The envelope is spiraling in towards the disk at a rate of $\sim 4.2 \times 10^{-6} M_{\odot} \text{ yr}^{-1}$ ⁽²⁰⁾. This high infall rate is consistent with fast accretion within the disk through GI-driven spirals that transport angular momentum efficiently^{31,32}. In addition, a ring of envelope-disk accretion shock emission from the SO molecule has been detected around the outer edge of the disk⁵, providing strong evidence for mass accretion from the envelope onto the disk. Moreover, as discussed in Methods, the millimeter continuum emission from the VLA 1 disk can be reasonably fitted with a simple flared disk model. The fit indicates the VLA 1 disk has a relatively high mass of 0.33-0.50 M_{\odot} , or 22%-33% of the protostellar mass. Therefore, the resulting Toomre's Q value is less than 1.5 for the outer part of the disk with a radius $\gtrsim 100$ au (Supplementary Figure 3), further supporting the possibility of global non-axisymmetric GI as the driver for the spiral arms³³. If GI is occurring in the massive VLA 1 disk, it must play an important

role in facilitating accretion by transporting angular momentum outward¹⁷.

The spirals in the VLA 1 disk could instead be raised by a planet or companion. Our fit of the Archimedean form to the spirals indicates the pitch angle increases inwards to ~ 40 au ($0''.1$), where we would thus expect the planet or companion to be located and to clear a gap in the disk. However, since the disk seems to be too massive for a planet to open a gap detectable at the current resolution³⁴, observations at higher resolution are needed to search for a gap and check for this scenario. In addition, since it has been suggested that the spiral arms in Elias 2-27 are due to a so-far undetected external companion in the disk plane¹¹, it is natural to ask whether the spiral arms in the VLA 1 disk can also be driven by an external companion. One possibility is VLA 2, but we believe this is not likely to be the driver because the disk of VLA 1 is highly inclined with respect to the plane of the sky, being nearly edge-on. If VLA 2 lies on the disk plane of VLA 1, it would have to be located at a distance much larger than its projected separation of $\sim 1,200$ au, which would greatly reduce its gravitational influence on the VLA 1 disk. If VLA 2 is located far from the VLA 1 disk plane, in addition to inducing spiral arms it should warp the disk. No sign of warping is detected in our continuum observations; higher resolution continuum and especially line observations are desirable to put tighter constraints on any disk warping. Another possibility is a putative stellar companion of $\sim 1M_{\odot}$, inferred to lie at a distance of ~ 186 au from VLA 1 based on the wiggling of the HH 111 jet and counterjet³⁵. However, such a massive young star should have a disk detectable with our sensitive ALMA continuum observation if it is at an evolutionary stage similar to that of VLA 1, yet nothing is seen. Further observations are needed to check the possibility that a companion in a suitable position has been missed.

1. Bate, M. R. Collapse of a Molecular Cloud Core to Stellar Densities: The First Three-dimensional Calculations. *Astrophys. J. Lett.* **508**, L95-L98 (1998)
2. Rice, W. K. M., Armitage, P. J., Bate, M. R., & Bonnell, I. A. The effect of cooling on the global stability of self-gravitating protoplanetary discs. *Mon. Not. R. Astron. Soc.* **339**, 1025-1030 (2003)
3. Tomida, K., Machida, M. N., Saigo, K., Tomisaka, K., & Matsumoto, T. Exposed Long-lifetime First Core: A New Model of First Cores Based on Radiation Hydrodynamics. *Astrophys. J. Lett.* **725**, L239-L244 (2010)
4. Harsono, D., Alexander, R. D., & Levin, Y. Global gravitational instabilities in discs with infall. *Mon. Not. R. Astron. Soc.* **413**, 423-433 (2011)
5. Lee, C.-F., Hwang, H.-C., & Li, Z.-Y. Angular Momentum Loss in the Envelope-Disk Transition Region of the HH 111 Protostellar System: Evidence for Magnetic Braking?. *Astrophys. J.* **826**, 213 (2016)
6. Pérez, L. M., Carpenter, J. M., Andrews, S. M., et al. Spiral density waves in a young protoplanetary disk. *Science* **353**, 1519-1521 (2016)
7. Andrews, S. M., Huang, J., Pérez, L. M., et al. The Disk Substructures at High Angular Resolution Project (DSHARP). I. Motivation, Sample, Calibration, and Overview. *Astrophys. J. Lett.* **869**, L41 (2018)

8. Huang, J., Andrews, S. M., Pérez, L. M., et al. The Disk Substructures at High Angular Resolution Project (DSHARP). III. Spiral Structures in the Millimeter Continuum of the Elias 27, IM Lup, and WaOph 6 Disks. *Astrophys. J. Lett.* **869**, L43 (2018)
9. Kurtovic, N. T., Pérez, L. M., Benisty, M., et al. The Disk Substructures at High Angular Resolution Project (DSHARP). IV. Characterizing Substructures and Interactions in Disks around Multiple Star Systems. *Astrophys. J. Lett.* **869**, L44 (2018)
10. Hall, C., Rice, K., Dipierro, G., Forgan, D., Harries, T., & Alexander, R. Is the spiral morphology of the Elias 2-27 circumstellar disc due to gravitational instability?. *Mon. Not. R. Astron. Soc.* **477**, 1004-1014 (2018)
11. Meru, F., Juhász, A., Ilee, J. D., Clarke, C. J., Rosotti, G. P., & Booth, R. A. On the Origin of the Spiral Morphology in the Elias 2-27 Circumstellar Disk. *Astrophys. J. Lett.* **839**, L24 (2017)
12. Forgan, D. H., Ilee, J. D., & Meru, F. Are Elias 2-27's Spiral Arms Driven by Self-gravity, or by a Companion? A Comparative Spiral Morphology Study. *Astrophys. J. Lett.* **860**, L5 (2018)
13. Toomre, A. On the gravitational stability of a disk of stars. *Astrophys. J.* **139**, 1217-1238 (1964)
14. Gammie, C. F. Nonlinear Outcome of Gravitational Instability in Cooling, Gaseous Disks. *Astrophys. J.* **553**, 174-183 (2001)
15. Tobin, J. J., Kratter, K. M., Persson, M. V., et al. A triple protostar system formed via fragmentation of a gravitationally unstable disk. *Nature* **538**, 483-486 (2016)

16. Alves, F. O., Girart, J. M., Caselli, P., Franco, G. A. P., Zhao, B., Vlemmings, W. H. T., Evans, M. G., & Ricci, L. Molecular outflow launched beyond the disk edge. *Astron. Astrophys.* **603**, L3 (2017)
17. Tomida, K., Machida, M. N., Hosokawa, T., Sakurai, Y., & Lin, C. H. Grand-design Spiral Arms in a Young Forming Circumstellar Disk. *Astrophys. J. Lett.* **835**, L11 (2017)
18. Turner, N. J., Fromang, S., Gammie, C., Klahr, H., Lesur, G., Wardle, M., & Bai, X.-N. in *Protostars and Planets VI*, (eds Beuther, H. et al.) 411-432 (Univ. Arizona Press, 2014)
19. Froebrich, D. Which Are the Youngest Protostars? Determining Properties of Confirmed and Candidate Class 0 Sources by Broadband Photometry. *Astrophys. J. Suppl.* **156**, 169-177 (2005)
20. Lee, C.-F. A Change of Rotation Profile in the Envelope in the HH 111 Protostellar System: A Transition to a Disk?. *Astrophys. J.* **725**, 712-720 (2010)
21. Reipurth, B., Bally, J., & Devine, D. Giant Herbig-Haro Flows. *Astron. J.* **114**, 2708 (1997)
22. Lee, C.-F. A Rotating Disk in the HH 111 Protostellar System. *Astrophys. J.* **741**, 62 (2011)
23. Lee, C.-F., Li, Z.-Y., Ching, T.-C., Lai, S.-P., & Yang, H. ALMA Dust Polarization Observations of Two Young Edge-on Protostellar Disks. *Astrophys. J.* **854**, 56 (2018)
24. Shu, F. H., Najita, J. R., Shang, H., and Li, Z.-Y. in *Protostars and Planets IV*, (eds Mannings, V. et al.) 789-814 (Univ. Arizona Press, 2000)
25. Konigl, A. & Pudritz, R. E. in *Protostars and Planets IV*, (eds Mannings, V. et al.) 759-787 (Univ. Arizona Press, 2000)

26. Sewifo, M., Wiseman, J., Indebetouw, R., Charnley, S. B., Pineda, J. E., Lindberg, J. E., & Qin, S.-L. Very Large Array Ammonia Observations of the HH 111/HH 121 Protostellar System: A Detection of a New Source with a Peculiar Chemistry. *Astrophys. J.* **849**, 68 (2017)
27. Reipurth, B., Raga, A. C., & Heathcote, S. Structure and Kinematics of the HH 111 Jet. *Astrophys. J.* **392**, 145 (1992)
28. Bae, J., & Zhu, Z. Planet-driven Spiral Arms in Protoplanetary Disks. II. Implications. *Astrophys. J.* **859**, 119 (2018)
29. Hall, C., Dong, R., Rice, K., Harries, T. J., Najita, J., Alexander, R., & Brittain, S. The Temporal Requirements of Directly Observing Self-gravitating Spiral Waves in Protoplanetary Disks with ALMA. *Astrophys. J.* **871**, 228 (2019)
30. Hennebelle, P., Lesur, G., & Fromang, S. Spiral-driven accretion in protoplanetary discs. II. Self-similar solutions. *Astron. Astrophys.* **590**, A22 (2016)
31. Dong, R., Hall, C., Rice, K., & Chiang, E. Spiral Arms in Gravitationally Unstable Protoplanetary Disks as Imaged in Scattered Light. *Astrophys. J. Lett.* **812**, L32 (2015)
32. Hall, C., Forgan, D., Rice, K., Harries, T. J., Klaassen, P. D., & Biller, B. Directly observing continuum emission from self-gravitating spiral waves. *Mon. Not. R. Astron. Soc.* **458**, 306-318 (2016)
33. Durisen, R. H., Boss, A. P., Mayer, L., Nelson, A. F., Quinn, T., & Rice, W. K. M. in *Protostars and Planets V* (eds Reipurth, B. et al.) 607-622 (Univ. Arizona Press, 2007)

34. Baruteau, C., & Masset, F. Type I Planetary Migration in a Self-Gravitating Disk. *Astrophys. J.* **678**, 483-497 (2008)
35. Noriega-Crespo, A., Raga, A. C., Lora, V., Stapelfeldt, K. R., & Carey, S. J. The Precession of the Herbig-Haro 111 Flow in the Infrared. *Astrophys. J. Lett.* **732**, L16-L20 (2011)

Correspondence and requests for materials should be addressed to C.-F.L.

Acknowledgements This paper makes use of the following ALMA data: ADS/JAO.ALMA#2015.1.00037.S and 2017.1.00044.S. ALMA is a partnership of ESO (representing its member states), NSF (USA) and NINS (Japan), together with NRC (Canada), NSC and ASIAA (Taiwan), and KASI (Republic of Korea), in cooperation with the Republic of Chile. The Joint ALMA Observatory is operated by ESO, AUI/NRAO and NAOJ. C.-F.L. acknowledges grants from the Ministry of Science and Technology of Taiwan (MoST 107-2119-M-001-040-MY3) and the Academia Sinica (Investigator Award AS-IA-108-M01). Z.-Y.L. is supported in part by NSF grants AST-1716259, 1815784 and 1910106 and NASA grant 80NSSC18K1095. N.J.T.'s contribution was carried out at the Jet Propulsion Laboratory, California Institute of Technology, under contract with NASA and with the support of NASA grant 17-XRP17_2-0081.

Author Contributions C.-F. Lee led the project, analysis, discussion, and drafted the manuscript. Z.-Y. Li and N. J. Turner commented on the manuscript and participated in the discussion.

Competing interests The authors declare no competing financial interests.

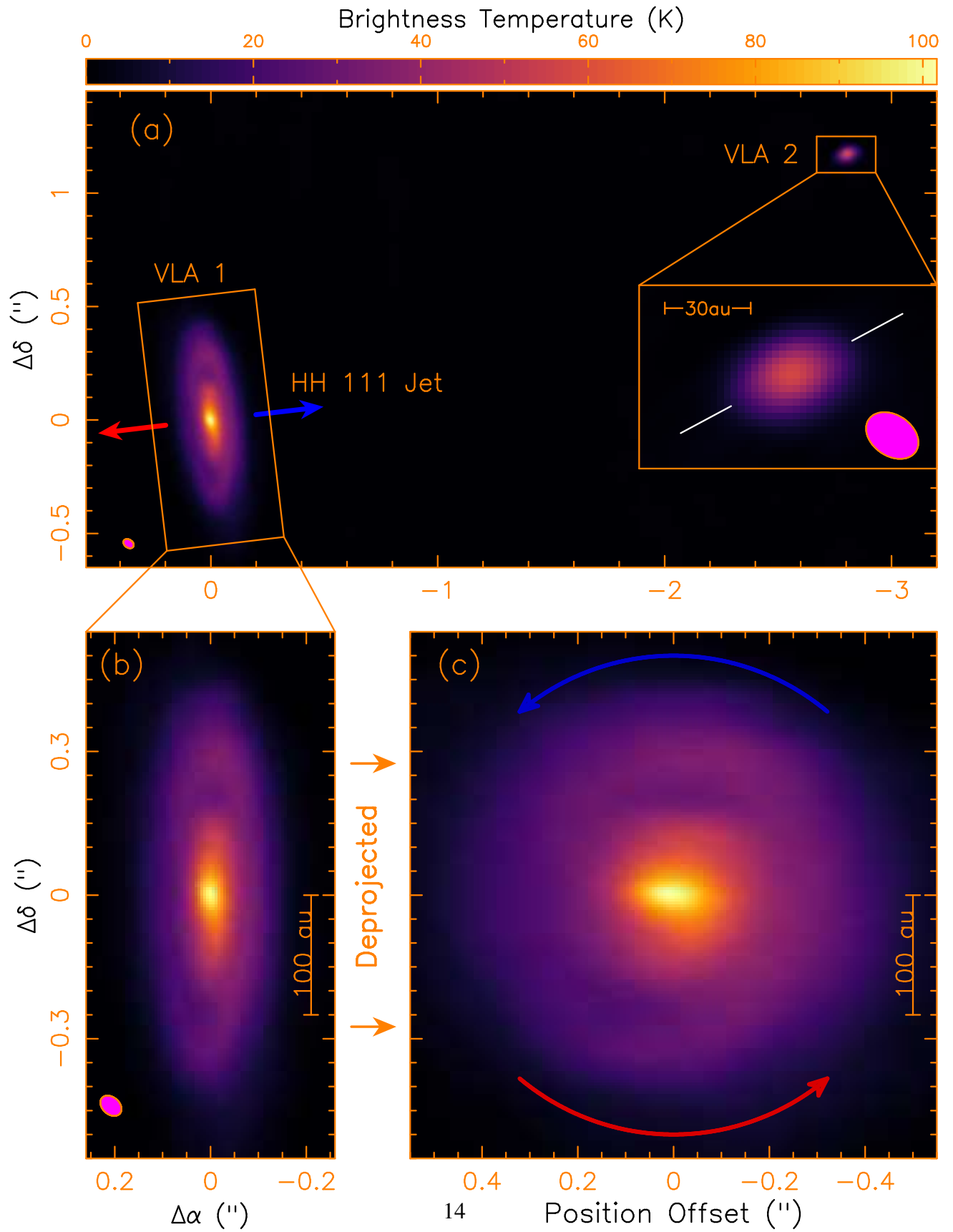


Figure 1. The 343 GHz continuum map towards the VLA 1 and 2 sources. The peak positions are ICRS $\alpha_{(2000)} = 05^{\text{h}}51^{\text{m}}46^{\text{s}}.2537$, $\delta_{(2000)} = +02^{\circ}48'29''.643$ and $\alpha_{(2000)} = 05^{\text{h}}51^{\text{m}}46^{\text{s}}.0665$, $\delta_{(2000)} = +02^{\circ}48'30''.815$, respectively for the VLA 1 and VLA 2 sources. The synthesized beam has a size of $0''.050 \times 0''.036$. Blue and red arrows in panel (a) indicate the orientations of the blueshifted (western) and redshifted (eastern) components of the HH 111 jet, respectively, emanating from the VLA 1 source. The inset is a zoom-in towards the VLA 2 source, with white lines marking the major axis of the continuum emission. Panel (b) shows a zoom-in on the disk around the VLA 1 source, rotated so the major axis is vertical. Panel (c) shows the VLA 1 disk deprojected by the inclination angle. Blue and red curved arrows show the direction of the disk rotation.

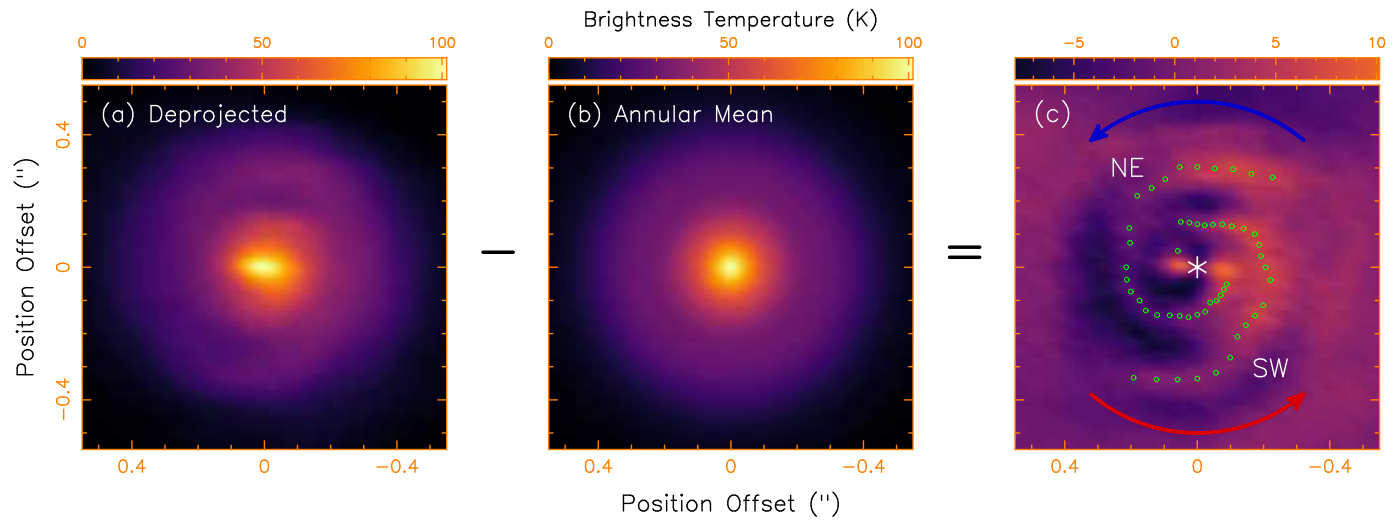


Figure 2. The spiral structure in the disk around the VLA 1 source. Panel (a) is the same as Figure 1c and shows the disk deprojected. In panel (b), the structure is annularly averaged.

Panel (c) shows the map obtained by subtracting the annular mean map from the deprojected map, revealing the underlying spiral features NE and SW, which have intensities $\sim 5\text{-}20\%$ of the local annular average. Blue and red curved arrows again show the direction of the disk rotation. Green open circles mark the emission peaks of the spirals, outlining the spiral features.

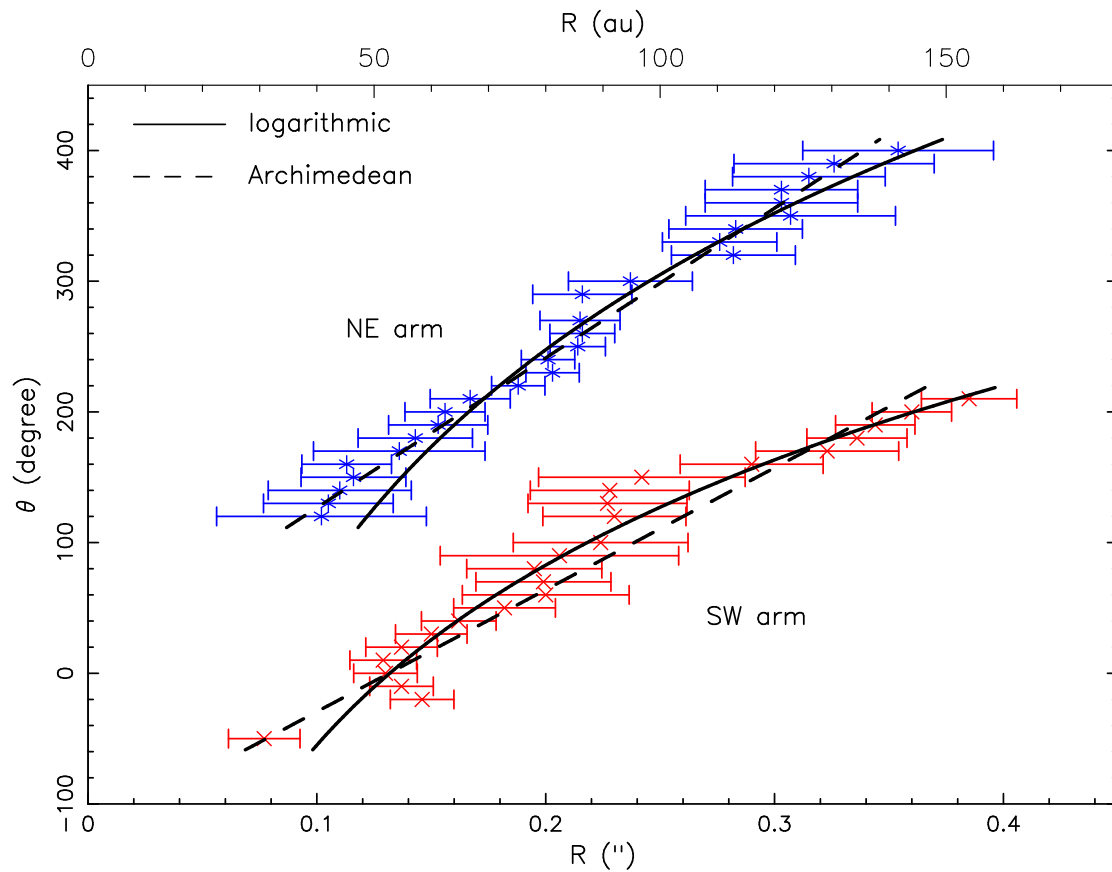


Figure 3. Two fits to each of the two spiral features in the VLA 1 disk. The NE and SW arm are offset vertically for clarity. Error bars show the arms' widths as measured by the Gaussians that best fit the emission intensities along rays from the central source. Each arm is fit in turn with a logarithmic (solid black curve) and an Archimedean spiral (dashed black curve).

Table 1. Best-Fit Logarithmic Spirals

Arm	R_0 (arcsecond)	a (radian ⁻¹)	χ^2	Pitch Angle (Degree)
SW	$0''.132 \pm 0''.003$	0.288 ± 0.010	2.07	$16.1^\circ \pm 0.6^\circ$
NE	$0''.077 \pm 0''.004$	0.222 ± 0.011	2.88	$12.5^\circ \pm 0.6^\circ$

Table 2. Best-Fit Archimedean Spirals

Arm	R_0 (arcsecond)	b (arcsecond radian ⁻¹)	χ^2	Pitch Angle [†] (Degree)
SW	$0''.132 \pm 0''.005$	0.061 ± 0.003	3.77	$23.4^\circ \pm 1.2^\circ - 8.8^\circ \pm 0.4^\circ$
NE	$-0''.011 \pm 0''.008$	0.050 ± 0.002	1.41	$19.1^\circ \pm 0.8^\circ - 7.2^\circ \pm 0.4^\circ$

†: Pitch Angle decreases from 60 au ($0''.15$) to 160 au ($0''.4$)

Methods

Observations We observed the HH 111 VLA 1 system with ALMA in Band 7 at ~ 343 GHz in Cycle 5 (Project ID: 2017.1.00044S). Three observations were carried out in C43-8 configuration using 47 antennas, two on 2017 November 28 and one on 2017 December 1, with a total time of ~ 109 minutes on target. The projected baseline lengths were ~ 60 -8550 meters. One pointing centered at the VLA 1 source was used. The primary beam (field of view) had a size of $\sim 17''.8$, covering both the VLA 1 and VLA 2 sources. The correlator was set to have four continuum windows, centered at 336.5, 338.5, 348.5, and 350.5 GHz for a total bandwidth of ~ 8 GHz. The maximum recoverable size (MRS) was $0''.54$. In order to restore a larger size scale, we combined these observations with our previous Cycle 3 observations²³, which had the same correlator setup but a larger MRS of $\sim 1''.4$. Thus, there is no noticeable missing flux in our maps of the disks around the two VLA sources, which have a size $\lesssim 1''$.

The CASA 5.1.1 package was used to calibrate the uv data obtained from our observations. Quasar J0510+1800 was observed as a passband calibrator and a flux calibrator, and quasar J0552+0313 (a flux of $\sim 0.24 \pm 0.10$ Jy) was observed as a gain calibrator. We also performed a phase-only self-calibration to improve the map fidelity. As mentioned above, we combined our observations with our previous Cycle 3 observations to avoid any missing flux for the disks. We used a super-uniform weighting with a robust factor of 0.25. The resulting synthesized beam (resolution) has a size of $0''.050 \times 0''.036$ at a position angle (P.A.) of $\sim 55^\circ$. The rms noise level is ~ 0.10 mJy beam⁻¹ (~ 0.58 K).

Spiral Structures Supplementary Figure 1 shows the spiral structures in the HH 111 VLA 1 disk presented in Figure 2c. We locate the emission peak positions of the spirals by fitting by eye a Gaussian to their emission intensity in the difference map cut along lines of constant position angle every 10° . Contours are also plotted outlining the spiral arms. The uncertainties in the peak positions are shown by radial error bars, marking the width at half maximum.

Disk Model Here we derive the properties of the VLA 1 disk in order to investigate the origin of the spiral structures. We adopt a parametrized flared disk model, the same as that used to reproduce the disk emission in the well-resolved Class 0 disk in HH 212³⁶. In this model, the disk is axisymmetric, with its physical parameters specified in cylindrical coordinates. It has a temperature

$$T = T_t \left(\frac{R}{R_t} \right)^{-q} \quad (1)$$

where R is the cylindrical radius, R_t is a representative radius to be defined below, T_t is the temperature at R_t , and q is the temperature power-law index. The model disk is in vertical hydrostatic equilibrium, with the number density of molecular hydrogen decreasing as a Gaussian in height above the midplane so

$$n = n_t \left(\frac{R}{R_t} \right)^{-p} \exp\left(-\frac{z^2}{2h^2}\right) \quad (2)$$

where n_t is the number density of molecular hydrogen in the midplane at R_t , p is the density

power-law index, and h is the scale height. The mass density is then $\rho = 1.4nm_{\text{H}_2}$, accounting for helium at solar abundance relative to hydrogen.

In vertical hydrostatic equilibrium, the scale height h comes from

$$\frac{h}{R} \sim \frac{c_s}{v_\phi} \propto \frac{R^{-q/2}}{R^{-1/2}} = R^{(1-q)/2} \quad (3)$$

where the isothermal sound speed $c_s \propto T^{1/2} \propto R^{-q/2}$. The rotation speed v_ϕ is Keplerian and thus given by $v_\phi = \sqrt{GM_*/R}$, where the protostellar mass $M_* \sim 1.5 M_\odot$, as found from the C^{18}O gas kinematics^{5,20}. With this scale height, increasing monotonically in radius, we failed to fit the observed thinning of the disk near its outer edge. Thus, as in HH 212, we assume the disk to be geometrically thinner near its outer edge. This could come from self-shielding reducing the temperature and thus the scale height in the outermost parts³⁷. Therefore, we define R_t to be the radius beyond which the scale height decreases towards the outer radius of the disk R_o . Thus, the scale height becomes

$$h(R) \sim h_t \begin{cases} \left(\frac{R}{R_t}\right)^{1+(1-q)/2} & \text{if } R < R_t, \\ \sqrt{1 - \frac{3}{4}\left(\frac{R-R_t}{R_o-R_t}\right)^2} & \text{if } R_t \leq R \leq R_o \end{cases} \quad (4)$$

where $h_t \sim \frac{c_s(R_t)}{v_\phi(R_t)}R_t$ is the scale height at R_t and $h = h_t/2$ at $R = R_o$.

For the dust continuum emission of the disk, we assume the dust opacity law

$$\kappa_\nu = 0.1 \left(\frac{\nu}{10^{12}\text{Hz}} \right)^\beta \text{ cm}^2 \text{ g}^{-1} \quad (5)$$

which has been used before for circumstellar disks in Taurus³⁸. Here β is the dust opacity spectral index and κ_ν the opacity per gram of gas and dust for a gas-to-dust mass ratio of 100. The β value is uncertain, affecting the disk mass needed to produce the observed total flux. To be inclusive, we consider values ranging from 0.6 as in the young HH 212 protostellar disk³⁶ to 1.0 as in protoplanetary disks^{38,39}. Therefore, we have $\kappa_\nu \sim 0.054 - 0.035 \text{ cm}^2 \text{ g}^{-1}$ at the observing frequency of 343 GHz.

To compute the dust emission, we tilt the model disk so its axis is $\sim 18^\circ$ from the plane of the sky, as estimated from the observed aspect ratio. We then compute the dust emission assuming local thermodynamic equilibrium, and integrate along a grid of lines of sight the local emission that is attenuated by the optical depth, as done before for the HH 212 disk³⁶. We then convolve the resulting map with the telescope's beam, producing a model map to be compared with the observed map at the same resolution.

Supplementary Figure 2 shows our best-fit continuum map. The model has 6 free parameters: R_t , R_o , q , T_t , p , and n_t . In our fit, $R_t \sim 0''.4$ (160 au), consistent with the observed radius of the disk, and $R_o \sim 0''.5$ (200 au) in order to produce the faint emission in the outer edge. The temperature power-law index $q \sim 0.55 \pm 0.11$, similar to that found in protoplanetary disks in Ophiuchus³⁹. With $T_t \sim 68 \pm 13 \text{ K}$, the resulting scale height h_t is approximately $0''.068 \pm 0''.007$ ($\sim 27 \pm 3 \text{ au}$) at R_t . For the density, we have $p \sim 1.5 \pm 0.4$ and $n_t \sim (6.0 - 9.3) \times 10^9 \text{ cm}^{-3}$ corre-

sponding to the range of opacities $\kappa \sim 0.054 - 0.035 \text{ cm}^2 \text{ g}^{-1}$. As can be seen in Supplementary Figure 2a, the model emission contours (red) can roughly match the observed emission contours (black with a gray-scaled image) of the continuum. Since the model is axisymmetric and does not include any spiral structures, we can not fit the non-axisymmetries. However, since the residuals are reasonably small (Supplementary Figure 2b), the model adequately describes the radial structure. In addition, as can be seen in Supplementary Figure 2c, since the model disk emission is mostly optically thick along the major axis, the temperature in our model is well constrained. In our model, the disk has a surface density

$$\Sigma = 1.4 m_{\text{H}_2} \int_{-\sqrt{2}h_t}^{\sqrt{2}h_t} n dz \quad (6)$$

and a mass

$$M_D = \int^{R_o} \Sigma 2\pi R dR \sim (0.33 - 0.50) M_{\odot} \quad (7)$$

which is $\sim 22\% - 33\%$ of the protostellar mass. Thus the disk is relatively massive.

Supplementary Figure 3 shows the model's stability against GI as measured by Toomre's Q parameter

$$Q \sim \frac{c_s \Omega}{\pi G \Sigma} \quad (8)$$

where $\Omega = \frac{v_\phi}{R}$ is the angular velocity of the disk. As can be seen, Q is less than 1.5 for $R \gtrsim 0''.25$ (100 au), indicating that the disk is gravitationally unstable in its outer half. Since the dust opacity is uncertain, further observations are needed to confirm the instability and check whether the inner part is also gravitationally unstable.

If the Q parameter at a given location were much less than unity, the scale height there would be dominated by the local self-gravity rather than the tidal gravity of the central star. The scale height would then be roughly⁴⁰:

$$h_s \sim \frac{c_s^2}{\pi G \Sigma} \sim Qh \quad (9)$$

The scale height would be significantly less than h . However, in our model, the Q parameter is of order unity or larger, and the effect of self-gravity on the scale height is moderate (at most a factor of 2).

Data availability. This letter makes use of the following ALMA data: ADS/JAO.ALMA2015.1.00037.S and 2017.1.00044.S. The data that support the plots within this paper and other findings of this study are available from the corresponding author upon reasonable request.

36. Lee, C.-F., Li, Z.-Y., Ho, P. T. P., Hirano, N., Zhang, Q., & Shang, H. First detection of equatorial dark dust lane in a protostellar disk at submillimeter wavelength. *Sci. Adv.* **3**, e1602935 (2017)

37. Dullemond, C. P., & Dominik, C. Flaring vs. self-shadowed disks: The SEDs of Herbig Ae/Be stars. *Astron. Astrophys.* **417**, 159-168 (2004)
38. Beckwith, S. V. W., Sargent, A. I., Chini, R. S., & Guesten, R. A Survey for Circumstellar Disks around Young Stellar Objects. *Astron. J.* **99**, 924-945 (1990)
39. Andrews, S. M., Wilner, D. J., Hughes, A. M., Qi, C., & Dullemond, C. P. Protoplanetary Disk Structures in Ophiuchus. *Astrophys. J.* **700**, 1502-1523 (2009)
40. Spitzer, L. The Dynamics of the Interstellar Medium. III. Galactic Distribution. *Astrophys. J.* **95**, 329-344 (1942)